Paper:

Designing and Modeling of Coanda Drone for Controllability

Ryo Shimomura*, Shin Kawai, and Hajime Nobuhara*****

Intelligent Interaction Technologies
Graduate School of Systems and Information Engineering
University of Tsukuba
1-1-1 Tennoudai, Tsukuba, Ibaraki, 305-8573 Japan
*E-mail: shimomura@cmu.iit.tsukuba.ac.jp
**E-mail: kawai@cmu.iit.tsukuba.ac.jp
***E-mail: nobuhara@iit.tsukuba.ac.jp

Abstract. This study proposes an aircraft design that can enable the development of a safe coanda drone without exposing the propeller. In the previously proposed coanda drone design, there is no external force in the yaw axis direction in the linear approximation model; therefore, the model is not controllable. This study proposes redesigning the propulsion mechanism that had previously been designed to be perpendicular to the ground to enable effective control of the yaw axis. The state equation derived shows that the airframe redesigned is controllable. The angle of the propulsion mechanism was changed at an interval of 15 degrees in the range 15–60 degrees, and the difference in response at that time was compared and verified through the simulation experiments conducted. This study shows that the redesigned coanda drone is controllable and useful in future control system designs. Since payload is important in drone systems, it was often assumed that tilting the thrust mechanism of the drone should be minimized; however, the results presented herein show that tilting of the thrust mechanism is not a significant issue from the viewpoint of mobility.

Keywords: Drone, UAV, UAS, Design, Modeling, Control, Coanda effect

1. Introduction

In recent years, multicopter type drones starting with AR drone often comprises multiple propellers spreading explosively [1, 2]. Since multicopter type drones are easy to operate and cost effective, they are currently being used in several fields, such as aerial photography, transportation, pesticide spraying, disaster response [3], medical practice [4], and forest observation [5]. In addition to applications in various fields, examples of patent applications relating to the use of drones are becoming popular [6]. As drones are increasingly used in several fields, danger, particularly that of exposure to propellers, is becoming a major concern. Since drones include propellers rotating at high speed, the risk of injury due to contact is significantly high even if the drone just flies close to the people. While the drone's fall from above is also dangerous, the presence of a rotating propeller at that time may increase the damage and lead to a more serious accident. Since the propeller of a large drone increases in proportion with the size of the drone, the safety of the operator and the surroundings during operation should be ensured. With the proliferation of drones in recent years, the risk of drone's falls and contacts is expected to increase. To solve these problems, we have previously proposed a safe drone design (hereinafter referred to as coanda drone) using the coanda effect which does not expose the propeller [8]. The coanda effect is a phenomenon by which a viscous fluid with a high velocity draws in the surrounding fluid. By using this phenomenon, the coanda drone attempts to fly at a flow rate greater than the flow rate observed inside of the aircraft. The coanda drone eliminates the exposure of propellers, which has been considered dangerous in previous multicopter drone systems and improves the safety of drones in the event of contact or fall. In addition to the inclusion of the propeller, the coanda effect has been applied to cope with the reduction in propulsion owing to the inclusion of the propeller. The coanda drone discussed in this paper refers to the propulsion mechanism design of the coanda drone optimized proposed in our previous study [8]. The purpose of this study is to present a way of designing a controllable coanda drone by redesigning the aircraft in such a way that the propulsion mechanism would be tilted to realize yaw control that ensures simple flight control of the coanda drone. Because stabilizing the aircraft via the controller only is quite complicated and sometimes may result in accidents when the aircraft shape is changed, which was not expected initially [9], it is crucial to design the drone with a focus on the control system design. Therefore, modeling the redesigned coanda drone is very important and cannot be overemphasized. While thrust is distributed circularly in the propulsion mechanism in the coanda drone, it is difficult to design due to the distributed thrust required when designing its control system. Therefore, for simplicity of the model, a model that assumes a distributed thrust as a plurality of thrust points is proposed. This study makes

it possible to realize a safe coanda drone with a simple control system.

2. Equations of motion

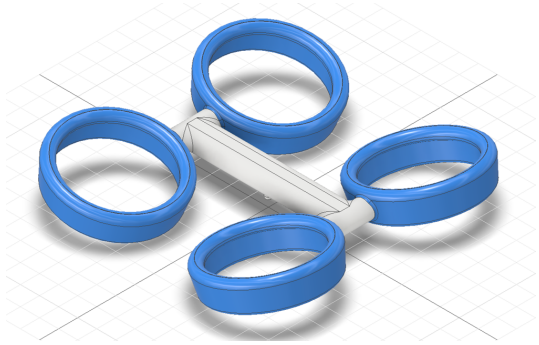

Fig. 1. New Coanda Drone Image

This paper focuses on the coanda drone design, which is outlined in figure 1. This section presents the coordinate system needed to describe the motion of the proposed coanda drone. Furthermore, the position vector of the point generating the thrust of the propulsion mechanism is also presented. In this study, we used the three coordinate systems shown in figure 2. The first coordinate system is a right-handed inertial coordinate system $\hat{F}^{\mathrm{i}}$ fixed to the ground with a certain reference point on the ground as the origin. In this paper, this coordinate system is referred to as a fixed coordinate system. The unit vectors $\hat{i}^{\mathrm{i}}, \hat{j}^{\mathrm{i}}$, and $\hat{k}^{\mathrm{i}}$ of the fixed coordinate system $\hat{F}^{\mathrm{i}}$ in each axis direction take the north direction, the east direction, and the vertical direction in the positive direction, respectively. The second coordinate system is a right-hand moving coordinate system $\hat{F}^{\mathrm{b}}$ fixed to the body with the center of gravity of the body as its origin. In this paper, this coordinate system is referred to as a body coordinate system. However, to simplify the moment of inertia tensor, each axis of this coordinate system can be aligned with the principal axis of inertia. The unit vectors $\hat{i}^{\mathrm{b}}, \hat{j}^{\mathrm{b}}$, and $\hat{k}^{\mathrm{b}}$ in each axial direction of the body coordinate system $\hat{F}^{\mathrm{b}}$ take the forward direction of the airframe, the rightward direction of the airframe, and the downward direction of the airframe, respectively, in a positive direction. The third coordinate system considered is the coordinate system $\hat{F}^{\mathrm{n}}$ used for navigation, which has the same origin as the fixed coordinate system. In this paper, this coordinate system is referred to as a navigation coordinate system. The unit vectors $\hat{i}^{\mathrm{n}}, \hat{j}^{\mathrm{n}}$, and $\hat{k}^{\mathrm{n}}$ in each axis direction of the navigation coordinate system $\hat{F}^{\mathrm{n}}$ assume the positive directions of north, east, and up. The transformation of each coordinate system can be performed as follows. First, the conversion from the fixed coordinate system to the body coordinate system would be presented. Herein, we consider a vector represented in the fixed coordinate system $\hat{F}^{\mathrm{i}}$ and the body coordinate system $\hat{F}^{\mathrm{b}}$ as $\begin{bmatrix} x^{\mathrm{i}} & y^{\mathrm{i}} & z^{\mathrm{i}} \end{bmatrix}^{\mathrm{T}}$, $\begin{bmatrix} x^{\mathrm{b}} & y^{\mathrm{b}} & z^{\mathrm{b}} \end{bmatrix}^{\mathrm{T}}$, respectively, where $\cdot^{\mathrm{T}}$ represents a transposition of a vector or matrix. The relationship between the two vectors can be expressed using the rotation matrix R, Figures 2 and 3 show the parameters, signals, and the body coordinate system of the aircraft. The four circles in the figure 2, $\mathrm{C}_1, \mathrm{C}_2, \mathrm{C}_3, \mathrm{C}_4$, represent the propulsion mechanism using the coanda effect. As described above, we considered an approximate thrust in this paper. These thrust forces are represented by $f_{i,1}, f_{i,2}, f_{i,3}, f_{i,4}$ for each C_i. Similarly, the point at which four thrusts exist in each propulsion mechanism is defined as $\mathrm{T}_{i,j}$, and the center of each propulsion mechanism C_i is defined as $\mathrm{O}_i^{\mathrm{c}}$.

The position vector in the body coordinate system of each point $\mathrm{T}_{i,j}$ generating thrust was obtained for use in the derivation of the external force moment in the equation of motion,. As mentioned above, the propulsion mechanism rotates about the axis in the $\hat{i}^{\mathrm{b}}$ direction through the center of each propulsion mechanism to obtain yaw direction input. First, it is assumed that the propulsion mechanism C_1 is not rotated about the axis in the $\hat{i}^{\mathrm{b}}$ direction. Herein, the point corresponding to the rotated $\mathrm{T}_{1,1}$ is defined as $\mathrm{T}'_{1,1}$. Next, the propulsion mechanism C_1 is rotated about an axis parallel to the $\hat{i}^{\mathrm{b}}$ axis.

3. Linear Model Approximation and its Analysis

In this section, we present an analysis based on the linear approximation and the linear approximation model of the derived state equation. A linear approximation of the state equation can be examined by considering the motion of the aircraft near the operating point. First, in 3.1, we derive an operation point which is a state in the neighborhood where the motion of the airframe is examined. Next, in 3.2, we derive a linear approximation established in the neighborhood of the operation point. Finally, 3.3 describes the controllability of the derived linear approximation model.

3.1. Derivation of the Operating Point

In this paper, we derive the operating point $(\boldsymbol{x}_e, \boldsymbol{u}_e)$ of the aircraft by considering the motion of a small displacement from its hovering state. Here, $\boldsymbol{x}_e = \boldsymbol{0}$. Thus, $\boldsymbol{f}(\boldsymbol{x}_e, \boldsymbol{u}(t))$ can be expressed as

$$\boldsymbol{f}(\boldsymbol{x}_e, \boldsymbol{u}(t)) = \begin{bmatrix} 0 \\ S_\eta \left(u_2(t) + u_3(t)\right) \\ M_{\mathrm{B}} g - C_\eta u_1(t) \\ \alpha_5 u_2(t) + \alpha_6 u_3(t) \\ \beta_5 u_4(t) + \beta_6 u_5(t) \\ \gamma_5 u_6(t) + \gamma_6 u_7(t) \\ 0 \\ 0 \\ 0 \\ 0 \\ 0 \\ 0 \end{bmatrix}. \tag{1}$$

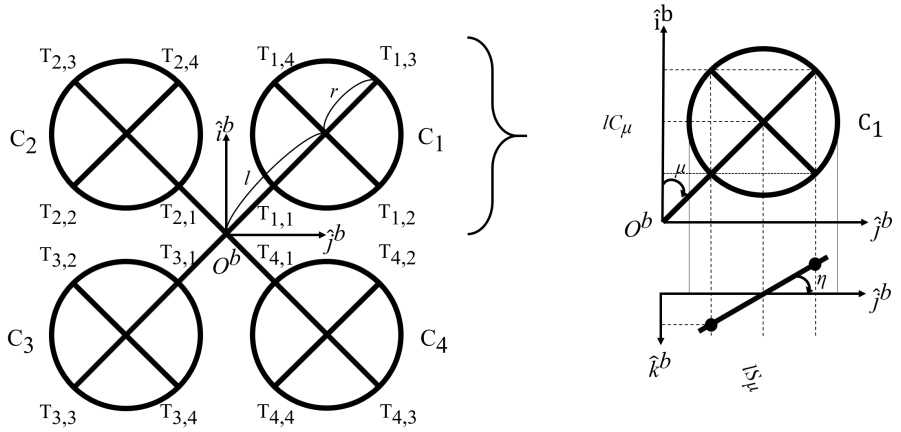

Fig. 2. Parameters and the Body Coordinate

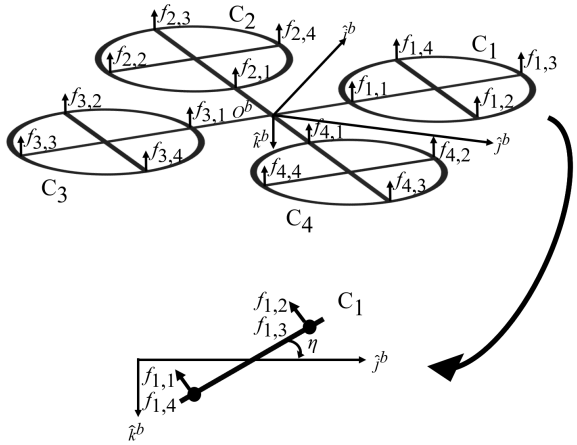

Fig. 3. Signals and the Body Coordinate

In this case, the input $\boldsymbol{u}(t)$, where the given expression is $\mathbf{0}^{\mathrm{T}}$, is $\boldsymbol{u}_e$. That is, the solution of the following simultaneous algebraic equations is the control input $\boldsymbol{u}_e$ of the operating point. M_{B} denotes the mass of the coanda drone.

$$S_\eta\left(u_2(t)+u_3(t)\right)=0, \tag{2}$$
$$C_\eta u_1(t)=M_{\mathrm{B}}g, \tag{3}$$
$$\alpha_5 u_2(t)+\alpha_6 u_3(t)=0, \tag{4}$$
$$\beta_5 u_4(t)+\beta_6 u_5(t)=0, \tag{5}$$
$$\gamma_5 u_6(t)+\gamma_6 u_7(t)=0. \tag{6}$$

From the structure of symmetry of the airframe, $f_{1,i}(t)=f_{2,i}(t)=f_{(}t)=f_{3,i}(t)=f_{4,i}(t)$ can be regarded as the solution of the simultaneous algebraic equations. At this time, $u_i(t)=0, i=\{2,3,4,5,6,7\}$, and the expressions (2) and (4) – (6) can be said to hold. Finally, from equation (3), $u_1(t)=M_{\mathrm{B}}g/C_\eta$ is the solution of the simultaneous algebraic equations. Therefore, the operating point of the aircraft can be expressed as

$$\boldsymbol{x}(t)=\boldsymbol{x}_e=\mathbf{0}, \tag{7}$$
$$\boldsymbol{u}(t)=\boldsymbol{u}_e=\begin{bmatrix}\frac{M_{\mathrm{B}}g}{C_\eta} & 0 & \dots & 0\end{bmatrix}^{\mathrm{T}}. \tag{8}$$

3.2. Linear Approximation

In the neighborhood of the derived operating point, the model can be approximated linearly as

$$E''\frac{d}{dt}\Delta\boldsymbol{x}(t)=A'\Delta\boldsymbol{x}(t)+B'\Delta\boldsymbol{u}(t), \tag{9}$$

where $\Delta\boldsymbol{x}(t),\Delta\boldsymbol{u}(t)$ denote differences from the operation points. $\Delta\boldsymbol{x}(t)=\boldsymbol{x}(t)-\boldsymbol{x}_e,\Delta\boldsymbol{u}(t)=\boldsymbol{u}(t)-\boldsymbol{u}_e$. In addition, E'',A',B' can be expressed as

$$E''=E'\big|_{\substack{\boldsymbol{x}(t)=\boldsymbol{x}_e,\\ \boldsymbol{u}(t)=\boldsymbol{u}_e}}=\begin{bmatrix}M_{\mathrm{B}}I_3 & \mathbf{0} & \mathbf{0} & \mathbf{0}\\ \mathbf{0} & J_{\mathrm{B}}^{\mathrm{b}} & \mathbf{0} & \mathbf{0}\\ \mathbf{0} & \mathbf{0} & I_3 & \mathbf{0}\\ \mathbf{0} & \mathbf{0} & \mathbf{0} & M_{\hat{k}}\end{bmatrix}, \tag{10}$$
$$A'=\left(a'_{ij}\right),B'=\left(b'_{ij}\right), \tag{11}$$
$$a'_{ij}=\left.\frac{\partial f_i\left(\boldsymbol{x}(t),\boldsymbol{u}(t)\right)}{\partial x_j}\right|_{\substack{\boldsymbol{x}(t)=\boldsymbol{x}_e,\\ \boldsymbol{u}(t)=\boldsymbol{u}_e}}, \tag{12}$$
$$b'_{ij}=\left.\frac{\partial f_i\left(\boldsymbol{x}(t),\boldsymbol{u}(t)\right)}{\partial u_j}\right|_{\substack{\boldsymbol{x}(t)=\boldsymbol{x}_e,\\ \boldsymbol{u}(t)=\boldsymbol{u}_e}}. \tag{13}$$

In this case, because the matrix E'' is non-singular, the state equation can be obtained by multiplying its inverse matrix from the left sides of the equations. Also, for the prediction of the expression, $\boldsymbol{x}(t),\boldsymbol{u}(t)$ can be rewritten as $\boldsymbol{x}(t)\coloneqq\Delta\boldsymbol{x}(t),\boldsymbol{u}(t)\coloneqq\Delta\boldsymbol{u}(t)$.

$$\frac{d}{dt}\boldsymbol{x}(t)=A\boldsymbol{x}(t)+B\boldsymbol{u}(t), \tag{14}$$

where A, B can be expressed as

$$A = E'^{-1}A' \tag{15}$$

$$= \begin{bmatrix}
0 & 0 & 0 & 0 & 0 & 0 & 0 & -g & 0 & 0 \\
0 & 0 & & & & & & & & \\
0 & 0 & 0 & 0 & 0 & 0 & g & 0 & 0 & 0 \\
0 & 0 & & & & & & & & \\
0 & 0 & 0 & 0 & 0 & 0 & 0 & 0 & 0 & 0 \\
0 & 0 & & & & & & & & \\
0 & 0 & 0 & 0 & 0 & 0 & 0 & 0 & 0 & 0 \\
0 & 0 & & & & & & & & \\
0 & 0 & 0 & 0 & 0 & 0 & 0 & 0 & 0 & 0 \\
0 & 0 & & & & & & & & \\
0 & 0 & 0 & 0 & 0 & 0 & 0 & 0 & 0 & 0 \\
0 & 0 & & & & & & & & \\
0 & 0 & 0 & 1 & 0 & 0 & 0 & 0 & 0 & 0 \\
0 & 0 & & & & & & & & \\
0 & 0 & 0 & 0 & 1 & 0 & 0 & 0 & 0 & 0 \\
0 & 0 & & & & & & & & \\
0 & 0 & 0 & 0 & 0 & 1 & 0 & 0 & 0 & 0 \\
0 & 0 & & & & & & & & \\
1 & 0 & 0 & 0 & 0 & 0 & 0 & 0 & 0 & 0 \\
0 & 0 & & & & & & & & \\
0 & 1 & 0 & 0 & 0 & 0 & 0 & 0 & 0 & 0 \\
0 & 0 & & & & & & & & \\
0 & 0 & -1 & 0 & 0 & 0 & 0 & 0 & 0 & 0 \\
0 & 0 & & & & & & & &
\end{bmatrix},$$

$$B = E'^{-1}B' \tag{16}$$

$$= \begin{bmatrix}
0 & 0 & 0 & 0 & 0 & 0 & 0 \\
0 & S_\eta/M_\mathrm{B} & S_\eta/M_\mathrm{B} & 0 & 0 & 0 & 0 \\
-C_\eta/M_\mathrm{B} & 0 & 0 & 0 & 0 & 0 & 0 \\
0 & \alpha_5/J_x & \alpha_6/J_x & 0 & 0 & 0 & 0 \\
0 & 0 & 0 & \beta_5/J_y & \beta_6/J_y & 0 & 0 \\
0 & 0 & 0 & 0 & 0 & \gamma_5/J_z & \gamma_6/J_z \\
0 & 0 & 0 & 0 & 0 & 0 & 0 \\
0 & 0 & 0 & 0 & 0 & 0 & 0 \\
0 & 0 & 0 & 0 & 0 & 0 & 0 \\
0 & 0 & 0 & 0 & 0 & 0 & 0 \\
0 & 0 & 0 & 0 & 0 & 0 & 0 \\
0 & 0 & 0 & 0 & 0 & 0 & 0
\end{bmatrix}.$$

3.3. Controllability Analysis

The purpose of this paper is to evaluate whether the above derived model, equation is controllable or not. Therefore, the controllability of the model can be ascertained by checking the controllability matrix. As a result, we confirmed from the rank condition of the controllability matrix that the linear approximation model is controllable with $\eta \neq 0$.

4. Simulation

In this section, the effect of the parameter η on the state equation of linear approximation is investigated. First, in section 4.1, a control system applied to a linear approximation model is presented to facilitate comparison based on simulation experiments. Next, 4.2 presents the results of the simulation conducted.

4.1. Control System Design

In this paper, the optimal control based linear quadratic regulator (LQR) and linear quadratic integral (LQI) control method were selected as a control system for comparison [13, 14]. Because the controllable parameter η distributes thrust in both horizontal and vertical directions, its effect is expected to appear as a trade-off between payload and attitude control. Therefore, it has been pointed out that the control target in the simulation needs to follow the step reference input in terms of altitude and yaw angle while maintaining hovering ability. Therefore, two optimal control methods: LQR and LQI control, were used together. For optimal control of the LQR or LQI control, a weight matrix of an evaluation function needs to be specified as a design parameter. It should be noted that it is necessary to make the values of this weight matrix common regardless of the value of η. By doing so, the difference in the simulation results depends only on the parameter η, and it has been reported that the influence of the parameter η can be easily examined by comparing the responses. For the design of LQR and LQI control systems, the derived linear approximation of the state equation is decomposed into two subsystems Σ_1, Σ_2. That is, there are two subsystems, $x^\mathrm{n}(t), y^\mathrm{n}(t), \phi(t), \theta(t)$, Σ_1 for LQR control, and $z^\mathrm{n}(t), \psi(t)$, Σ_2 for LQI control. The LQR and LQI control systems are designed for these two subsystems, respectively. Fortunately, the derived linear approximation of the state equation can be decomposed into two independent subsystems, Σ_1, Σ_2, which do not interfere with each other, as follows.

$$\Sigma_1 : \begin{cases} \dfrac{d}{dt}\boldsymbol{x}_1(t) = A_1\boldsymbol{x}_1(t) + B_1\boldsymbol{u}_1(t), \\ \boldsymbol{y}_1(t) = C_1\boldsymbol{x}_1(t), \end{cases} \tag{17}$$

$$\Sigma_2 : \begin{cases} \dfrac{d}{dt}\boldsymbol{x}_2(t) = A_2\boldsymbol{x}_2(t) + B_2\boldsymbol{u}_2(t), \\ \boldsymbol{y}_2(t) = C_2\boldsymbol{x}_2(t), \end{cases} \tag{18}$$

For these subsystems, the control structures of LQR and LQI are shown as figures 5 and 4. The gains of each controller, K_1, K_2, can be obtained as solutions of the optimization problems by minimizing the following evaluation functions, J_1, J_2, respectively.

$$J_1 = \int_0^\infty \left(\boldsymbol{x}_1(t)^\mathrm{T} Q_1 \boldsymbol{x}_1(t) + \boldsymbol{u}_1(t)^\mathrm{T} R_1 \boldsymbol{u}_1(t)\right) dt, \tag{19}$$

$$J_2 = \int_0^\infty \left(\boldsymbol{z}(t)^\mathrm{T} Q_2 \boldsymbol{z}(t) + \boldsymbol{u}_2(t)^\mathrm{T} R_2 \boldsymbol{u}_2(t)\right) dt, \tag{20}$$

where $\boldsymbol{z}(t)$ is $\boldsymbol{z}(t) = \begin{bmatrix}\boldsymbol{x}_2(t)^\mathrm{T} & \boldsymbol{e}(t)^\mathrm{T}\end{bmatrix}^\mathrm{T}, \boldsymbol{e}(t) = \boldsymbol{r}(t) - \boldsymbol{y}(t)$ and $\boldsymbol{r}(t)$ is a reference input. For simplicity, in this paper, Q_1, R_1, Q_2, R_2 are used as unit matrices of appropriate dimensions.

4.2. Simulation Results

Simulations were performed using Matlab and Simulink with the reference input $\boldsymbol{r}(t)$ as a step input

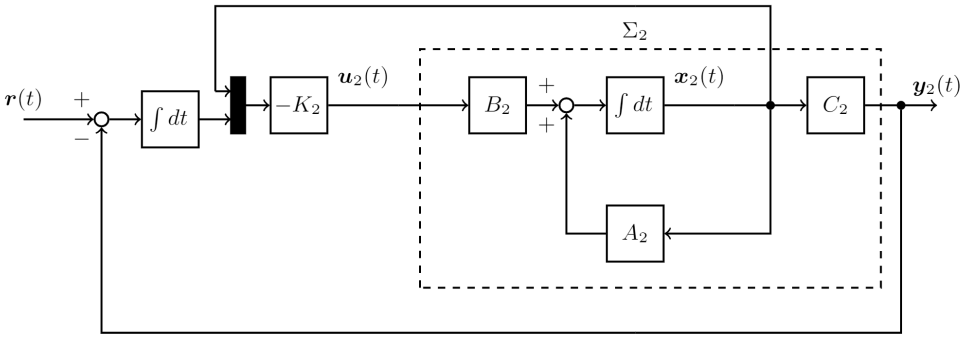

Fig. 4. Block Diagram: Σ_2 with LQI

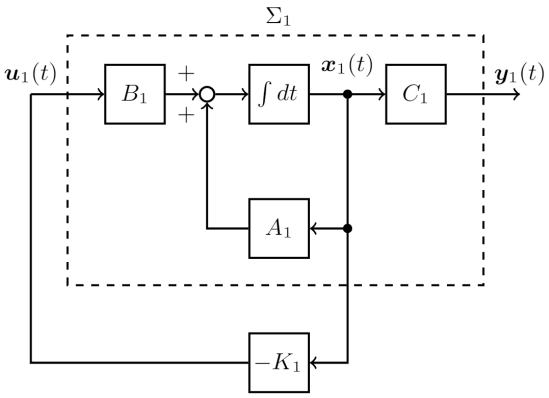

Fig. 5. Block Diagram: Σ_1 with LQR

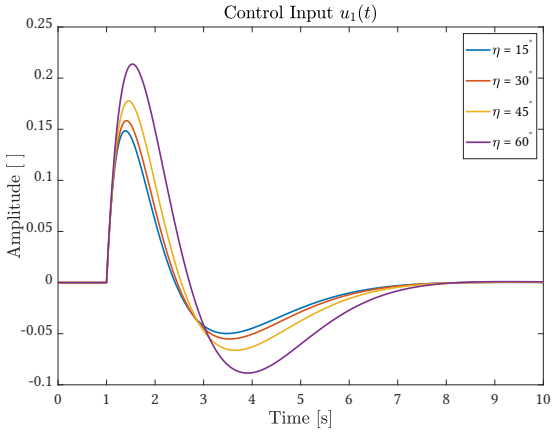

Fig. 6. Input 1 $u_1(t)$

without setting the disturbance and the initial condition of the coanda drone.

Further, four parameters of η for enabling control, $\eta = \{15°, 30°, 45°, 60°\}$, were used. However, because $\eta = 0$ (case of the coanda drone designed in a previous study [8]) cannot be compared under the same conditions as $\eta \neq 0$, a case of $\eta = 0$ is not carried out in this study. In this paper, while the control results of different values of η are compared by using the same evaluation function in designing control systems such as LQR, in the case of $\eta = 0$, the linear approximation model is uncontrollable and the LQR or LQI control system cannot be designed. Therefore, if $\eta = 0$, it cannot be compared under the same conditions as $\eta \neq 0$, so simulation under such condition was not conducted. At this point, the designed control gains K_1, K_2 with respect to η are as follows.

The simulation was conducted under the following settings. Simulation results are shown in figures 6 – 10. Figures 6 and 9 show the input $u_1(t)$ and output $z^n(t)$ of subsystem Σ_2, respectively. Figures 7 and 8 show inputs $u_6(t)$ and $u_7(t)$ of subsystem Σ_2, and figure 10 shows the output $\psi(t)$.

5. Conclusions

In this study, we succeeded in creating a controllable model by tilting the ejection mechanism of coanda drone. The controllability of the proposed design was confirmed by deriving the state equation of coanda drone's model. A simulation model was prepared using 3DCAD and the simulation experiment was conducted using MATLAB. In the simulation, we confirmed that the model is easier to control by changing the η angle. Because the proposed coanda drone is a safe drone that is not susceptible to the danger of propeller exposure, the coanda drone can be considered to be less likely to be damaged when the coanda drones collide with one another; also, the probability of a fall is low. A drone with a low probability of fall can be said to be very robust when used as a field robot. Further, it is expected that future drone usage will not be limited to one or two drones, but will involve the simultaneous operation of a large number of drones. In such a case, a coanda drone can be very useful. Moreover, the high safety of coanda drones implies they can be operated in urban areas and can be deployed very easily for applications such as logistics, infrastructure, and disaster response. They are expected to bring a significant social impact in terms of improved time efficiency in perform-

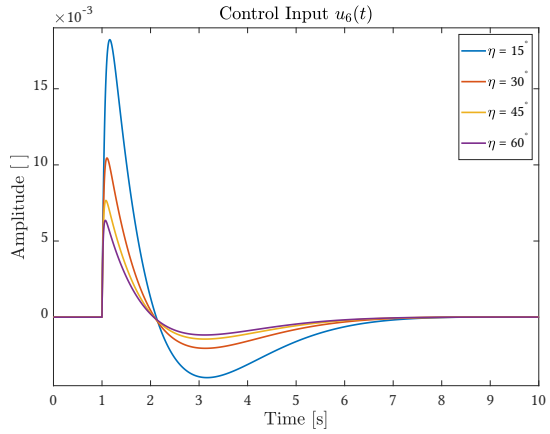

Fig. 7. Input 2 $u_6(t)$

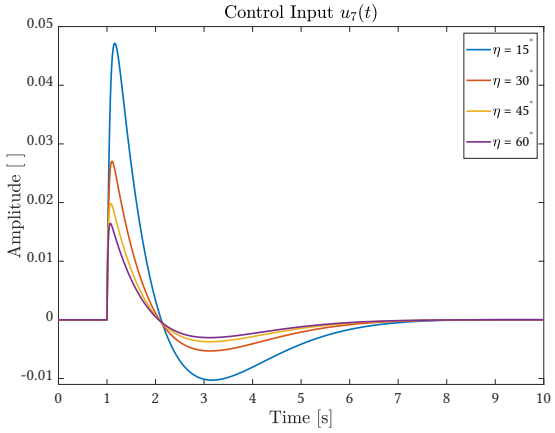

Fig. 8. Input 3 $u_7(t)$

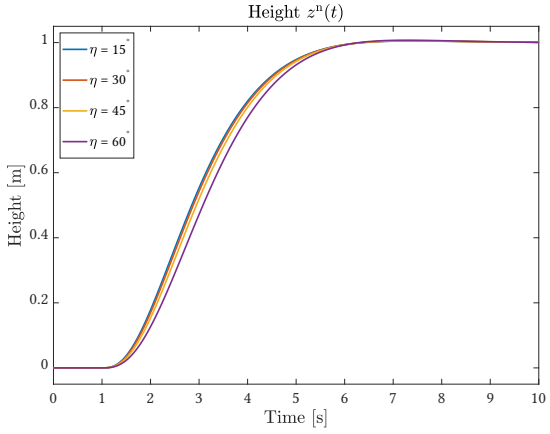

Fig. 9. Output 1 $z^{n}(t)$

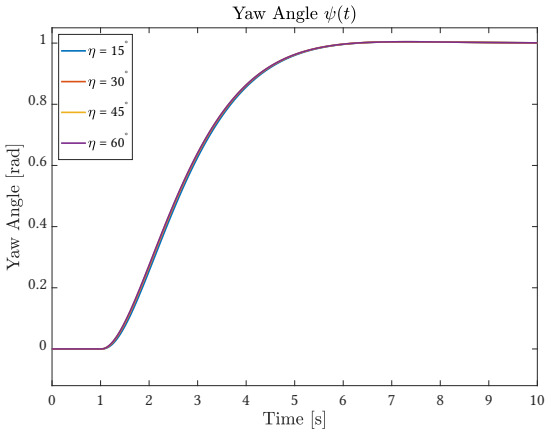

Fig. 10. Output 2 $\psi(t)$

ing work and replacement of human being in performing dangerous work.

Acknowledgements

This work was supported by JST CREST, Japan (grant no. JPMJCR1512).

References:

[1] P. Bristeau, F. Callou, D. Vissière and N. Petit, "The Navigation and Control technology inside the AR.Drone micro UAV," *2011 The International Federation of Automatic Control (IFAC)*, vol. 44, pp. 1477–1484, 2011.

[2] T. Krajník, V. Vonásek, D. Fišer and J. Faigl, "AR-Drone as a Platform for Robotic Research and Education," *Research and Education in Robotics - EUROBOT 2011*, pp. 172–186, 2011.

[3] P. Neumann, M. Bartholmai, J. H. Schiller, B. Wiggerich and M. Manolov, "Micro-drone for the characterization and self-optimizing search of hazardous gaseous substance sources: A new approach to determine wind speed and direction," *2010 IEEE International Workshop on Robotic and Sensors Environments*, pp. 1–6, 2010.

[4] E. Judy and H. Carlton, "Models for Drone Delivery of Medications and Other Healthcare Items," *Unmanned Aerial Vehicles: Breakthroughs in Research and Practice*, pp. 376–392, 2019.

[5] L. P. Koh and S. A. Wich, "Dawn of Drone Ecology: Low-Cost Autonomous Aerial Vehicles for Conservation," *Tropical Conservation Science*, vol. 5, no. 2, pp 121–132, 2012.

[6] Tyco Fire and Security GmbH, "Drone Tours In Security Systems," *Patent Application Publication in United States*, 2014.

[7] "Flyability," `https://www.flyability.com/`

[8] R. Shimomura, S. Kawai, H. Nobuhara, "Designing a Safe Drone with the Coanda Effect Based on a Self-Organizing Map," *2018 IEEE International Conference on Systems, Man, and Cybernetics (SMC)*, pp. 4171–4177, 2018.

[9] Gregory Travis, "How the Boeing 737 Max Disaster Looks to a Software Developer," *IEEE Spectrum*, 2019.

[10] E. Bernard, "Dynamics of Atmospheric Flight," *Dover Books on Aeronautical Engineering*, 2012.

[11] G. Strang, "Introduction to Linear Algebra," *Wellesley-Cambridge Press*, 2016.

[12] M. Elad, "Sparse and Redundant Representations: From Theory to Applications in Signal and Image Processing," *Springer New York*, 2010.

[13] K. Ogata, "Modern Control Engineering," *Pearson*, 2010.

[14] P. C. Young and J. C. Willems, "An approach to the linear multivariable servomechanism problem," *International Journal of Control*, vol. 15, no. 5, pp. 961–979, 1972.